Large Longitude Libration of Mercury Reveals a Molten Core

J. L. Margot,[1]* S. J. Peale,[2] R. F. Jurgens,[3] M. A. Slade,[3] I. V. Holin[4]

Observations of radar speckle patterns tied to the rotation of Mercury establish that the planet occupies a Cassini state with obliquity of 2.11 ± 0.1 arc minutes. The measurements show that the planet exhibits librations in longitude that are forced at the 88-day orbital period, as predicted by theory. The large amplitude of the oscillations, 35.8 ± 2 arc seconds, together with the Mariner 10 determination of the gravitational harmonic coefficient C_{22}, indicates that the mantle of Mercury is decoupled from a core that is at least partially molten.

Because Mercury is an end-member planet, the characterization of its interior properties is crucial to further our understanding of the formation and evolution of habitable worlds. A question that has challenged planetary scientists for more than three decades is the state of Mercury's core (*1*). Determining the nature and extent of the core would enable progress in four fundamental areas. First, models of the internal structure of the planet have so far been constrained only by its mean density of 5.43 g cm^{-3} (*2*), with early (*3*) and recent (*4*) calculations yielding a wide range of possible internal configurations. Although it is generally accepted that the planet differentiated early into an iron core and a silicate mantle (*5*), improved descriptions of the mass distribution within the planet require the measurement of core properties or moments of inertia. Second, thermal evolution models (*6*) predict a core that is fully or partially liquid, or completely solid. The outcome is particularly sensitive to the abundance of a light alloying element in the core, presumably sulfur, that lowers the melting temperature and allows the maintenance of a liquid outer core over billions of years (*7*). In order to focus the thermal evolution calculations, the extent and state of the core must be determined. Third, a long-standing puzzle relates to the origin of the magnetic field that was measured by Mariner 10 at a strength of roughly 1% that of Earth (*8*). A dynamo mechanism involving motion in an electrically conducting molten core is the preferred explanation (*9*, *10*), but alternative theories that do not require a currently liquid core, such as remanent magnetism in the crust, cannot be ruled out (*11*, *12*). Finally, the presence of a liquid core may bear on the unusual spin-orbit configuration of Mercury. It has been suggested that increased energy dissipation at a core/mantle interface would lead to almost certain capture in specific spin-orbit resonances (*13*, *14*), although this capture can also occur naturally as a result of the chaotic evolution of the orbital eccentricity, without the need for additional core/mantle friction (*15*).

One of us (Peale) devised an observational procedure to characterize the size and state of the core of Mercury, and showed that it is possible to detect a molten core by measuring subtle deviations from the mean resonant spin rate of the planet (*1*). The early expectation was that the experiment would require landers on the surface of the planet. Here we describe how we have used Earth-based radar instruments to make high-precision measurements of the instantaneous spin rate, and we present observational evidence indicating that Mercury has a molten core. We also provide observational confirmation that Mercury occupies a Cassini state (*16*) and a measurement of the obliquity of the planet, both of which are required for further characterization of the core with Peale's formalism (*1*).

Since the discovery that the spin period of Mercury differs from its orbital period (*17*), it has been hypothesized that the planet rotates on its spin axis three times for every two revolutions around the Sun (*18*) and occupies a Cassini state, in which its spin vector is nearly perpendicular to the orbital plane and precesses at the same rate as the orbital plane (*14*). As Mercury follows its orbit with eccentricity $e \sim 0.206$, it experiences periodically reversing torques due to the gravitational influence of the Sun on the asymmetric figure of the planet. The torques affect the spin angular momentum and cause small deviations of the spin rate from its resonant value of 3/2 times the mean orbital frequency. The resulting oscillations in longitude are called forced librations, where the forcing and the rotational response occur with a period $P \sim 88$ days, dictated by the orbital motion. The physical librations are characterized by an angle ϕ (*14*) representing the deviations of the orientation of the planet from the exact resonant value

$$\phi = \frac{3}{2}\frac{(B-A)}{C} f(e)\sin(nt) \qquad (1)$$

where $A < B < C$ are the principal moments of inertia, $f(e)$ is a power series in the eccentricity, and $n = 2\pi/P$ is the orbital (forcing) frequency. The gravitational torques and resulting angular deviations are proportional to the difference in equatorial moments of inertia ($B - A$), a measure of the asymmetry in the mass distribution. The polar moment of inertia C appears in the denominator because it represents a measure of the resistance to changes in rotational motion. If the core of Mercury is solid and the entire planet participates in the librations, C is the relevant moment of inertia. However, if the mantle is decoupled from a fluid core that does not follow the librations, the appropriate moment of inertia in the denominator of Eq. 1 is that of the mantle alone C_m or, more precisely, mantle plus crust. Because $C_m/C \leq 0.5$ in all plausible interior models (*3*, *4*), the amplitude of the librations in the presence of a liquid core is twice as large as it would be with a solid core. Therefore, a measurement of the libration amplitude provides a straightforward mechanism for determining the state of the core remotely. The quantity ($B - A$) is known from Mariner 10 measurements of the second-degree and -order gravitational coefficient C_{22} (*2*)

$$C_{22} = \frac{(B-A)}{4MR^2} = (1 \pm 0.5) \times 10^{-5} \qquad (2)$$

where M and R are the mass and radius of the planet, respectively. The moment of inertia C/MR^2 has not been measured, but interior models constrain it to the range from 0.325 to 0.380 (*4*), where the smallest value corresponds to the most centrally condensed configuration (*19*). Using these data in Eq. 1 shows that the amplitude of the forced librations in the case of a solid core should be within 50% of 19 to 22 arc sec. The amplitude that we measured is outside this range, suggesting a liquid core.

Method. Radar echoes from solid planets exhibit spatial irregularities in the wavefront caused by the constructive and destructive interference of waves scattered by the irregular surface. Because of the rotation of the planet, the corrugations in the wavefront, also called speckles, will sweep over the receiving station and give rise to fluctuations of the electromagnetic signal with time. It is fruitful to evaluate the degree of correlation between signals received at one station located in spacetime at ($\mathbf{x}$, t) with respect to those received at another station at ($\mathbf{x} + \delta\mathbf{x}$, $t + \delta t$). The properties of this spacetime correlation function were first analyzed by Green (*20*, *21*), who showed that for some orientation of the baseline $\delta\mathbf{x}$, there exists a time delay δt at which the correlation maximizes. When the trajectory of the wavefront corruga-

[1]Department of Astronomy, Cornell University, 304 Space Sciences Building, Ithaca, NY 14853, USA. [2]Department of Physics, University of California, Santa Barbara, CA 93106, USA. [3]Jet Propulsion Laboratory, 4800 Oak Grove Drive, Pasadena, CA 91109, USA. [4]Space Research Institute, Moscow, Russian Federation.

*To whom correspondence should be addressed. E-mail: jlm@astro.cornell.edu

tions is parallel to the antenna baseline, the value of the time delay that maximizes the correlation is related in a simple fashion to the magnitude and orientation of the spin vector of the planet. Green (*21*) gives an expression valid to first order

$$|\delta \mathbf{x}| = 2r\Omega\cos(\alpha)\delta t_{\max} \quad (3)$$

where r is the range to the planet, Ω is the sidereal spin rate, and α is the tilt of the spin vector from perpendicularity with the line of sight.

That echoes received at two receivers can display a high degree of correlation under appropriate viewing geometry has been well known for some time in the radar astronomy community (*22*). But the power of the technique to measure planetary spin states was not fully appreciated until one of us (Holin) brought it to the attention of the rest of us in 2001. George (*23*) developed an expression for the cross-correlation function of the electric field scattered from a rough rotating sphere to two observation points. His formalism shows that speckles remain coherent over a rotation angle given approximately by $(\lambda/a)^{1/2}$, where λ is the wavelength and a is the radius of the sphere. For Earth-based observations of Mercury ($r \sim 100$ million km), it can be shown that the pattern of speckles remains frozen over a linear distance many times the radius of Earth (*24*, *25*). In practice, one illuminates the planet with monochromatic radiation and records the speckle pattern as it sweeps over two receiving stations. Because the wavefront corrugations are tied to the rotation of the planet, and because decorrelation of the speckle pattern can be neglected (*26*), the time lag obtained by cross-correlating the two echo time series yields a direct measurement of the instantaneous spin rate, as shown by Green's formula. The result holds for arbitrary topography (*27*).

A substantial requirement is that both receiving stations must record similar speckle patterns to produce a large correlation, and this can occur only when the trajectory of the speckles is aligned with the antenna baseline. The characteristic scale of the speckles is given by the classic diffraction formula $r\lambda/d$, where d is the size of the scattering patch on the surface, on the order of the planetary radius. This scale is small compared to the separation between antennas (~ 1 km versus ~ 3000 km in our experiment), so that a small (0.02°) misalignment of the speckle trajectory with respect to the baseline orientation results in appreciable decorrelation. For an east-west baseline that oscillates daily by ±23° with respect to the ecliptic, the high correlation condition is maintained each day for only ~20 s. This realization led one of us (Holin) to present results (*24*, *25*) showing that measurements of the epochs at which the correlation maximizes would provide tight constraints on the spin vector orientation. In practice, one makes use of the antenna spacetime locations that are known with great accuracy to derive the spin vector geometry. Because the time of day at which large correlations are observed is not particularly sensitive to α in Eq. 3, the experiment must be performed at multiple line-of-sight geometries to fully determine the direction of the spin axis in inertial space.

Observations. For most of our observations (Table 1) we used the NASA/Jet Propulsion Laboratory (JPL) 70-m antenna (DSS-14) at Goldstone, California (35.24°N, –116.89°E) and transmitted a circularly polarized monochromatic signal at a frequency of 8560 MHz (λ = 3.5 cm) and power of ~420 kW. Transmission typically occurred for the duration of the round-trip light time to the planet, and reception followed for an equivalent amount of time. Transmit times were carefully selected so that the daily maximum in the correlation would fall during a receive window. Radar echoes were recorded at Goldstone and at the Robert C. Byrd Green Bank Telescope (GBT) in West Virginia (38.24°N, –79.84°E) with fast sampling systems (*28*). Representative values of the signal-to-noise ratio (SNR) in the same (SC) and opposite (OC) circular polarizations as that transmitted were ~3 and ~20, respectively, in a 200-Hz bandwidth. Some of our observations made use of the Arecibo telescope in Puerto Rico (18.23°N, –66.75°E) as the transmitter (λ = 12.6 cm) and DSS-14 or a smaller 34-m antenna (DSS-13) as the receiver.

Complex cross-correlations (*29*) of the echo time series obtained at the receiving stations yield strong correlations near the predicted epochs. The time evolution of the rise and fall in the correlation is well approximated by a Gaussian curve (Fig. 1). For large SNRs, centroid locations can be determined with a precision that is a small fraction of the widths of the correlation functions (*30*). Epochs of correlation maximum and time lags can be determined to a precision of ~ 0.5 s and ~ 0.1 ms from initial widths of ~ 5 s and ~ 2.5 ms, respectively. Although the OC echo is dominated by a specular component representative of a smaller fraction of the planetary disk than that which produces the diffuse SC echo, measurements in the two receive polarizations exhibit a high degree of consistency.

Results. We used the epochs of correlation maximum (Table 1) in a least-squares fit to derive the position of the axis of rotation of Mercury in the J2000 equatorial frame (Fig. 2). Our calculations include the motions of the planets as given by the *JPL Planetary Ephemeris DE414* (*31*), an Earth orientation model incorporating up-to-date timing and polar motion data, time delays accounting for light-travel times, and general relativistic corrections to the time delays.

Table 1. Log of observations. Each data set identifier (ID) shows the date of observation in the format yymmdd followed by the frequency of observation (x = 8560 MHz and s = 2380 MHz), the observing stations involved (0 = DSS-14, 3 = DSS-13, G = GBT, and A = Arecibo), and the receive polarization (OC = opposite sense circular polarization to that transmitted; SC = same sense, not shown). The MJD gives the epoch of speckle correlation maximum, the centroid of a Gaussian of standard deviation w. The time lag (τ) indicates the time interval for speckles to travel from one station to the other at the corresponding epoch. The fractional uncertainty in the time lag and spin rate (σ) is empirically determined from successive measurements, except in the first four data sets, where it corresponds to a residual timing uncertainty of 0.2 ms. The last column indicates the instantaneous spin rate in units of 3/2 of the mean orbital frequency.

ID	MJD	w (s)	τ (s)	σ	Spin rate
020513x00Goc	52407.889680	4.41	–12.36958	1.61×10^{-5}	0.999985
020522x00Goc	52416.871258	6.27	–12.69218	1.58×10^{-5}	0.999893
020602x00Goc	52427.845539	5.98	–11.84078	1.69×10^{-5}	0.999861
020612x00Goc	52437.816052	6.35	–11.21227	1.78×10^{-5}	0.999945
030113x00Goc	52652.760205	10.32	–10.93565	1.37×10^{-5}	1.000097
030123x00Goc	52662.725791	8.40	–11.29540	5.28×10^{-6}	1.000073
030531x00Goc	52790.846925	7.76	–8.30671	8.21×10^{-6}	0.999932
030601x00Goc	52791.844164	7.37	–8.36904	1.02×10^{-5}	0.999949
030918sA3Aoc	52900.630649	26.79	–14.67124	5.03×10^{-5}	1.000093
030919sA3Aoc	52901.628954	28.95	–14.70674	5.50×10^{-5}	1.000065
030920sA3Aoc	52902.627306	26.94	–14.71705	5.18×10^{-5}	1.000067
040331x00Goc	53095.968346	5.92	–7.41574	1.20×10^{-5}	1.000098
041212x00Goc	53351.866334	7.86	–7.74059	1.55×10^{-5}	1.000070
041218x00Goc	53357.848521	7.75	–7.38323	1.05×10^{-5}	1.000067
041219x00Goc	53358.845401	8.13	–7.39330	9.67×10^{-6}	1.000075
050313x00Goc	53443.004320	7.04	–4.78491	3.19×10^{-5}	1.000035
050314x00Goc	53444.001094	6.87	–4.98779	9.83×10^{-6}	1.000056
050316x00Goc	53445.994761	6.72	–5.31606	1.45×10^{-5}	1.000047
050318x00Goc	53447.988621	6.24	–5.53562	1.52×10^{-5}	1.000056
060629x00Goc	53915.735467	8.03	–11.27627	8.35×10^{-6}	0.999866
060712x00Goc	53928.676641	7.94	–10.71493	6.43×10^{-6}	0.999882

The best spacecraft determination of the orientation of the rotation axis gives an obliquity of ~2° (with a 50% error ellipse of ±2.6° by ±6.5°) (*32*). The constraints obtained from previous Earth-based radar measurements are about 10 times better (*33*). Our measurements refine the knowledge of the pole orientation by two orders of magnitude. The measured obliquity is 2.11 ± 0.1 arc min, which is precisely within the range of theoretical expectations (*34*). Our adopted 1σ uncertainty exceeds the formal uncertainties of the fit to guard against undetected systematic effects.

Mercury is expected to be in a Cassini state in which its orbit pole, spin orientation, and perpendicular to the Laplacian plane remain coplanar (*14*). Numerical simulations (*35*, *36*) support this theoretical prediction. Our spin solution shows that, within observational errors, Mercury occupies Cassini state 1: The confidence regions for the spin orientation fall precisely on the locus of pole positions that satisfy the Cassini condition (Fig. 2). The latter condition relies on a numerical determination of the Laplacian plane (*35*) that is entirely independent of the radar data. If we use this Laplacian plane and assume that Mercury is in a Cassini state, the best-fit constrained pole solution is at J2000 right ascension 281.0097° and declination 61.4143°.

A detailed characterization of the core of Mercury in the manner described by Peale (*1*) requires not only the occupancy of the Cassini state but also a precise knowledge of the obliquity, amplitude of the librations, and second-degree gravitational harmonic coefficients. We provide observational confirmation that the first condition is satisfied and values for the first two quantities. Although current uncertainties on gravitational harmonic coefficients (*2*) prevent us from constraining the size of the core, it is possible to determine the state of the core by measuring the amplitude of the 88-day forced librations.

We determined the amplitude of the librations of Mercury by measuring the instantaneous spin rate of the planet at various epochs. Our fractional uncertainties, on the order of 1 part in 10^5, are such that the libration signature is readily apparent. In order to translate our time-lag measurements into values of the rotational velocity of Mercury at each observing epoch (Table 1), we fit for the spin rate value that best satisfies the coherence condition; namely, that the orientation of the planet as seen by the first transmitter-receiver pair at time t is similar to the orientation of the planet as seen by the second transmitter-receiver pair at time $t + \delta t_{max}$. This is accomplished by computing the trajectories of light rays between transmitter, bounce point, and receiver, taking light-travel times into account. A Lorentz transformation is used to obtain the orientation of the incoming and outgoing light rays in the moving frame in which Mercury is at rest. Those orientations are converted to planetocentric coordinates with the use of the appropriate rotation matrices. For each observation epoch, the spin rate is adjusted to minimize the difference between the longitudes corresponding to the first transmitter-receiver pair and the longitudes corresponding to the second transmitter-receiver pair, ensuring the coherence condition. Our measured angular velocities reliably trace the phase of the expected libration signature derived from the torque equation, indicating that the 88-day forced librations have been detected unambiguously (Fig. 3).

Results are very similar in the two circular polarizations. One-parameter fits to the spin rate variations, adjusting in a least-squares sense for the overall amplitude only, yield $(B - A)/C_m = (2.01 \pm 0.09) \times 10^{-4}$ and $(B - A)/C_m = (2.08 \pm 0.07) \times 10^{-4}$ with reduced chi-square (χ^2_ν) values of 2.3 and 1.3 for the OC and SC data, respectively. A fit to the combined OC and SC data yields $(B - A)/C_m = (2.04 \pm 0.06) \times 10^{-4}$, with $\chi^2_\nu = 1.8$. The best-fit libration amplitude is not sensitive to the exact spin vector orientation. All Cassini poles with obliquities spanning the range 2.11 ± 0.1 arc min yield consistent results.

To test for the presence of a long-period libration component superposed on the 88-day libration signature, we performed additional fits to the libration equation. A fully dynamical solution admits three free parameters: the overall amplitude, initial libration angle γ_0, and initial angular velocity $(d\gamma/dt)_0$, where we chose the 17 April 2002 perihelion passage [modified Julian date (MJD) 52381.480] as the initial epoch. The best-fit values ($\chi^2_\nu = 0.9$) to the combined OC and SC data are $(B - A)/C_m = (2.03 \pm 0.04) \times 10^{-4}$, $\gamma_0 = (0.07 \pm 0.01)°$, $(d\gamma/dt)_0 = (2.10 \pm 0.06)$ arc sec day^{-1}, corresponding to a long-period libration amplitude of ~300 arc sec. Because the data span less than a complete cycle, values for the long-period component need confirmation. The period of the free libration is $P \times \{3[(B - A)/(C_m)]\ (7e/2 - 123e^3/16)\}^{-1/2}$, or ~12 years (*37*).

Our adopted value of the moment ratio is $(B - A)/C_m = (2.03 \pm 0.12) \times 10^{-4}$, where the 1σ uncertainty captures the 1σ range of the OC-only and SC-only models. This corresponds to an amplitude of the forced librations $\phi = (35.8 \pm 2)$ arc sec. This value should be compared to the expected amplitude for a solid planet: ϕ within 50% of 19 to 22 arc sec for $C/MR^2 = 0.325$ to 0.380 (*4*) and $C_{22} = (1.0 \pm 0.5) \times 10^{-5}$ (*2*).

The large libration amplitude that we observe can be explained by a mantle that is decoupled

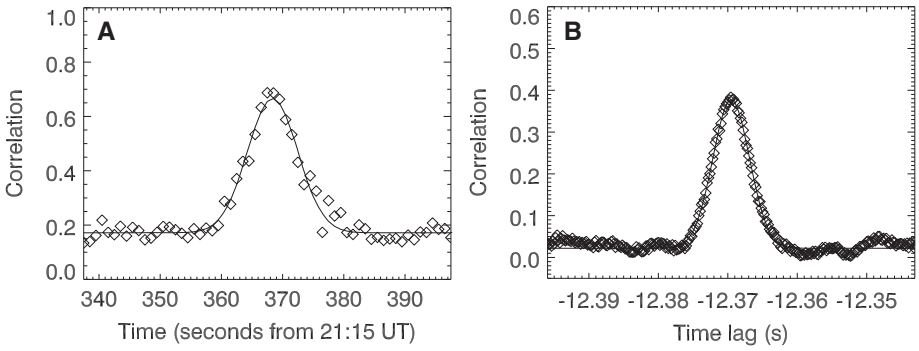

Fig. 1. Representative correlation functions obtained on the first observing run (13 May 2002) with integration times of 1 s (symbols) and corresponding Gaussian fits (solid lines). (**A**) Time evolution of the maximum in the cross-correlation function when using echo time series with 200-Hz sampling. The maximum in the function represents the epoch at which the speckle trajectory passes through both antenna spacetime locations. UT, universal time. (**B**) Cross-correlation of echo time series with 5000-Hz sampling at the time of the correlation maximum. Successive measurements of the Gaussian centroid were used to produce the time-lag estimates and fractional uncertainties listed in Table 1. Correlation is highest when the sampling rate matches about half the limb-to-limb bandwidth of the planet as in (A). Other sampling rates yield a lower SNR.

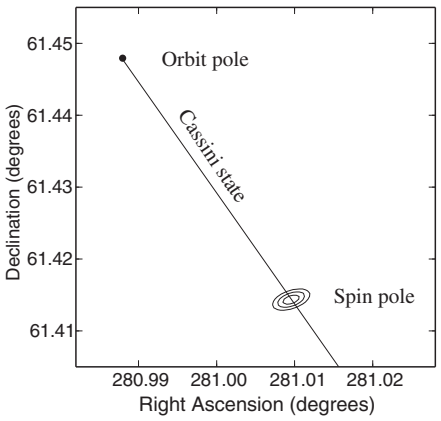

Fig. 2. Orientation of the spin axis of Mercury, based on the observed epochs of correlation maximum. The formal 68, 95, and 99% joint confidence regions for the spin orientation are shown as contours. The solution was not constrained to obey the Cassini state condition, which is represented by the straight solid line. The equatorial coordinate frame, pole orientations, and Cassini state locations all refer to the J2000 epoch.

from the core or by a serious underestimate of the C_{22} coefficient (*38*). To explain the nominal 35.8 arc sec libration amplitude with a solid core would require a C_{22} value at least 1.6 times larger than that obtained from Mariner 10 data. In the absence of any other constraint, one can estimate the probability of this occurring to be about 10%, assuming that errors are normally distributed. But because Mercury is in a Cassini state, an additional relationship exists between gravitational harmonic coefficients and obliquity (*14*). We can use this relationship with our obliquity determination to show that C_{22} values in excess of the nominal Mariner 10 range would require the quadrupole moment J_2 to also be outside the Mariner 10 range, a combination of circumstances with less than 10% probability.

In order to evaluate the impact of joint errors on the observables, we performed error propagation analysis and Monte Carlo simulations, where trial values for C_{22} and ϕ were drawn from normal distributions with mean and standard deviations corresponding to their measured values and error bars. We then computed the diagnostic ratio C_m/C (*39*) for extreme values of the moment of inertia allowed by interior models (*4*). The results (Fig. 4A) show that C_m/C is smaller than unity with 90% confidence, whereas a solid core requires $C_m/C = 1$. If one includes the additional constraint applicable in a Cassini state (Fig. 4B), the confidence level increases to 95%. The nominal $C_m/C \cong 0.5$ value implied by our measurements indicates that an outer shell participates alone in the librations, as opposed to the entire planet, and requires that the core of Mercury be at least partially molten.

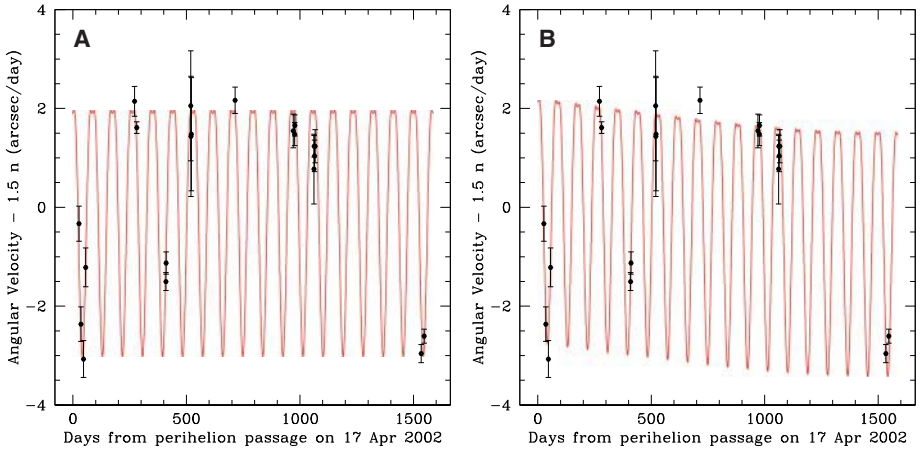

Fig. 3. Mercury spin rate deviations from the resonant rate of 3/2 times the mean orbital frequency. Observed data points and their error bars from Table 1 are shown at their respective epochs. The solid line is a numerical integration of the torque equation, the phase of which is dictated by the time of pericenter passage. (**A**) A one-parameter fit to the OC data (allowing for 88-day forced librations only). (**B**) A three-parameter fit to the OC data (allowing for an additional 12-year free libration component).

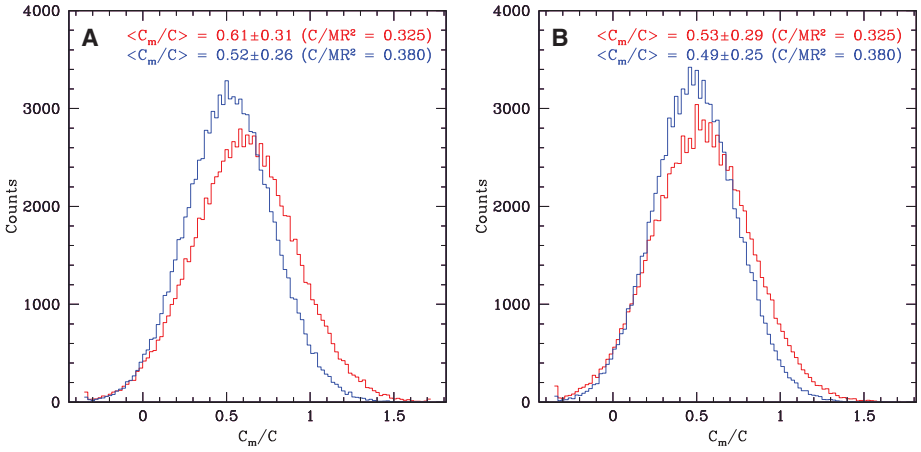

Fig. 4. Histograms of the diagnostic quantity C_m/C, where values less than unity indicate a liquid core, obtained by using 10^5 draws from normal distributions of ϕ and C_{22} values. Both extremes in the range of plausible interior models $C/MR^2 = 0.325$ (red) and $C/MR^2 = 0.380$ (blue) are considered. (**A**) shows the results without invoking the Cassini state, whereas (**B**) includes the additional constraint that exists between gravitational harmonic coefficients and obliquity in a Cassini state (*14*).

Implications. The presence of a magnetic field at Mercury (*8*) cannot be taken as observational evidence of a liquid core, because a currently active dynamo is not the only viable mechanism for producing the field (*11*, *12*). Our observations strengthen the dynamo hypothesis, in that a liquid core is a necessary condition for dynamo action. Although the sufficient conditions for a dynamo are not known, Stevenson (*10*) has shown that the existence of convection in a partially molten core, rather than the vigor of that convection, is the primary determinant. Thermal convection may arise if the heat flow exceeds the conductive heat flow that can be supported adiabatically. This will be facilitated by latent heat release if an inner core freezes. Inner core growth may also promote chemical convection as the freezing process excludes light alloying elements from the inner core, and as the material at the bottom of the outer core becomes compositionally buoyant because of an excess of those light elements. It is estimated that a fluid layer depth on the order of 100 km or more is required for sustaining convection by compositional buoyancy in Mercury (*10*). The effectiveness of dynamo processes in various geometries and whether such dynamos can reproduce the field observed by Mariner 10 are topics of active research. Simulations (*40*) indicate that some thin-shell dynamo configurations plausible for Mercury produce the observed field properties. Other geometries have been proposed, such as dynamos operating deeply underneath a stably stratified liquid outer core (*41*) or thick-shell dynamos (*42*). The MESSENGER spacecraft (*43*), en route to Mercury, is expected to map the magnetic field in detail and to determine the nature of its source (*44*).

The presence of a liquid core in Mercury has important implications for theories of planet formation and evolution. Thermal models predict a frozen core unless a sufficient amount of sulfur (at least 0.1% weight fraction) depresses the melting temperature of the core material (*6*). But chemical condensation models (*45*) indicate that sulfur cannot condense in the primordial solar nebula at the heliocentric distance of Mercury. Hence, the need for a sufficient amount of accreted sulfur to keep the core molten over the age of the solar system implies that Mercury was accreted from planetesimals that originated over a wide range of heliocentric distances. It may be possible to place further constraints on the amount of sulfur if it can be shown that the liquid core is convecting; that is, if it can be proven that a dynamo is responsible for the magnetic field. Although a minimum amount of sulfur is necessary to maintain a liquid core, too much sulfur inhibits inner core growth and core convection. If the sulfur abundance exceeds ~ 6 to 10% (*7*, *6*, *46*), the core would remain com-

pletely fluid over the age of the solar system, and a dynamo process would be unlikely.

Although the large amplitude of the forced librations indicates a liquid core, our observations cannot determine the size of the core, the extent of the inner core, or the polar moment of inertia of Mercury. These parameters are required to assemble a more complete picture of the internal structure of the planet and to probe the thermal evolution and magnetic field generation in much greater detail. Our error bars on C_m/C are currently dominated by uncertainties in the value of C_{22} (Fig. 4). But this gravitational harmonic can be constrained to the 1% level or better by tracking the orbit of a spacecraft. With such a measurement, expected from MESSENGER (*43*), our error bars on C_m/C would instantly drop to a level commensurate with uncertainties on the libration amplitude, roughly 6%. By assuming the densities of crust, mantle, and core material and using the integral relations for the ratio of moments of inertia, the C_m/C value could then be used to place a useful constraint on the size of the core. A superior estimate will require measurements of the polar moment of inertia of the planet (*1*, *14*, *34*, *39*), which can be derived by combining improved estimates of the gravitational harmonic coefficients with our values of the obliquity and libration amplitude.

Earth rotation studies demonstrate that the long-term monitoring of planetary rotations reveals excitations on a variety of time scales that can be used to constrain the underlying geophysical processes (*47*). The mechanisms affecting rotation also provide insights into interior structure, viscoelastic properties, and interactions at the core/mantle and atmosphere/surface boundaries. The capability to monitor the spins of terrestrial planets with Earth-based radar provides a new tool to probe the interiors of planets and opens new avenues in planetary physics.

References and Notes

1. S. J. Peale, *Nature* **262**, 765 (1976).
2. J. D. Anderson, G. Colombo, P. B. Esposito, E. L. Lau, G. B. Trager, *Icarus* **71**, 337 (1987).
3. R. W. Siegfried, S. C. Solomon, *Icarus* **23**, 192 (1974).
4. H. Harder, G. Schubert, *Icarus* **151**, 118 (2001).
5. C. Chapman, *Mercury*, F. Vilas, C. Chapman, M. Matthews, Eds. (Univ. of Arizona Press, Tucson, AZ, 1988), pp. 1–23.
6. G. Schubert, M. N. Ross, D. J. Stevenson, T. Spohn, *Mercury*, F. Vilas, C. Chapman, M. Matthews, Eds. (Univ. of Arizona Press, Tucson, AZ, 1988), pp. 429–460.
7. D. J. Stevenson, T. Spohn, G. Schubert, *Icarus* **54**, 466 (1983).
8. N. F. Ness, K. W. Behannon, R. P. Lepping, Y. C. Whang, K. H. Schatten, *Science* **185**, 151 (1974).
9. N. F. Ness, K. W. Behannon, R. P. Lepping, Y. C. Whang, *J. Geophys. Res.* **80**, 2708 (1975).
10. D. J. Stevenson, *Rep. Prog. Phys.* **46**, 555 (1983).
11. A. Stephenson, *Earth Planet. Sci. Lett.* **28**, 454 (1976).
12. O. Aharonson, M. T. Zuber, S. C. Solomon, *Earth Planet. Sci. Lett.* **218**, 261 (2004).
13. P. Goldreich, S. Peale, *Astron. J.* **72**, 662 (1967).
14. S. J. Peale, *Mercury*, F. Vilas, C. Chapman, M. Matthews, Eds. (Univ. of Arizona Press, Tucson, AZ, 1988), pp. 461–493.
15. A. C. M. Correia, J. Laskar, *Nature* **429**, 848 (2004).
16. A Cassini state is a stable dynamical configuration that is the result of tidal evolution. In this state, the spin axis remains coplanar with the orbit normal and the Laplacian plane normal as the former two precess around the latter from planetary perturbations of the orbit. The Laplacian plane is that plane about which Mercury's orbital plane precesses uniformly with a constant inclination.
17. G. H. Pettengill, R. B. Dyce, *Nature* **206**, 1240 (1965).
18. G. Colombo, *Nature* **208**, 575 (1965).
19. A uniform-density sphere has $C/MR^2 = 0.4$. Values for Earth and Mars are 0.331 and 0.366, respectively. The value for Venus has not been measured.
20. P. E. Green, *Radar Astronomy Measurement Techniques* (Technical Report 282, MIT Lincoln Laboratory, Lexington, MA, 1962).
21. P. E. Green, *Radar Astronomy* (McGraw-Hill, New York, 1968), chap. 1.
22. The property has been used to measure the topography of the Moon with receiving stations separated in space (*48*, *49*) or time (*50*) and led to the development of interferometric synthetic-aperture radar. On 31 January 1974, R. and S. Goldstein observed Venus with a Goldstone-Green Bank configuration and looked for a correlation between the two echo time series but did not detect it.
23. N. George, *J. Opt. Soc. Am.* **66**, 1182 (1976).
24. I. V. Kholin, *Radiophys. Quant. Elec.* **31**, 371 (1988) [translation from I. V. Holin, *Izv. Vyssh. Uchebn. Zaveden. Radiofiz.*, **31**, 515 (1988)].
25. I. V. Kholin, *Radiophys. Quant. Elec.* **35**, 284 (1992) [translation from I. V. Holin, *Izv. Vyssh. Uchebn. Zaveden. Radiofiz.*, **35**, 433 (1992)].
26. I. V. Kholin, *Solar System Res.* **38**, 449 (2004) [translation from I. V. Holin, *Astron. Vestnik* **38**, 513 (2004)].
27. An approximate expression for the field backscattered by a surface S can be written using the Fresnel-Kirchhoff diffraction formula (*50*): $E \propto \int_S \Gamma e^{-ik(r+s)} rsdS$, where E is the electric field, Γ is the complex reflection coefficient, $k = 2\pi/\lambda$, and r and s are the one-way distances for uplink and downlink. The cross-correlation of this echo with that received at a later time by a second receiving station is given by $\rho \propto \int_S \Gamma\Gamma^* e^{-ik(r+s-r'-s')} dS$, where geometric attenuation over the short observation time is assumed to be constant. Holin (*24*) demonstrated that if the surface is located in the Fresnel zone with respect to the source, the expression in parentheses can be reduced to a scalar product $\mathbf{r} \cdot \mathbf{x}$ where the first factor is the planetocentric surface location $\mathbf{r}$ and the second factor describes the motion but is independent of $\mathbf{r}$. If the condition $\mathbf{x} = 0$ is realized, contributions from individual scatterers add in phase and the correlation is large. This occurs when the translational and rotational components of the motion cancel in such a way that the speckle pattern observed at the first station is similar to that observed at the second station at a later time. Because the coherence condition is independent of $\mathbf{r}$, rotational parameters can be derived for arbitrarily shaped surfaces, as long as they exhibit diffuse scattering (*24*).
28. J. L. Margot, in *Proceedings of the 2002 URSI General Assembly*, paper 1949 (Maastricht, Netherlands, 2002).
29. We use $|E[x(t)y^*(t+\tau)]|$, where E is the expectation operator, and $x(t)$ and $y(t)$ are the complex voltage time series after demodulation to baseband.
30. J. S. Bendat, A. G. Piersol, *Random Data. Analysis and Measurement Procedures* (Wiley, New York, ed. 2, 1986).
31. E. M. Standish, *JPL Planetary Ephemeris DE414* (Technical Report IOM 343R-06-002, JPL, Pasadena, CA, 2006).
32. K. P. Klaasen, *Icarus* **28**, 469 (1976).
33. Initial radar images of the polar regions indicated that the component of the polar obliquity in the line-of-sight direction must be <1° (*52*). Improved images obtained 2 years later showed that the zero-obliquity case gave minimum smearing of the images (*53*). Further analysis showed a pole direction that yields a nominal obliquity of 0.5° (*53*).
34. S. J. Peale, R. J. Phillips, S. C. Solomon, D. E. Smith, M. T. Zuber, *Meteorit. Planet. Sci.* **37**, 1269 (2002).
35. M. Yseboodt, J. L. Margot, *Icarus* **181**, 327 (2006).
36. S. J. Peale, *Icarus* **181**, 338 (2006).
37. This is close to the orbital period of Jupiter, which may provide the required forcing. Another excitation mechanism is required if the long-period component is a true free libration that is not forced by Jupiter.
38. The C_{22} value was determined on the basis of the first and third Mariner 10 encounters, with different orbital inclinations (21.3° and 76.8°) and different close approach longitudes (99.9° at an altitude of 706 km and 52.2° at an altitude of 327 km). The Mariner 10 Radio Science team performed a careful analysis to arrive at realistic error bars. They concluded that "The resulting realistic errors, adjusted to include systematic effects, are about a factor of 10 larger than the formal errors on the gravity parameters."
39. The ratio $[(C_m)/(C)] = [(C_m)/(B-A)][(B-A)/(MR^2)][(MR^2)/(C)]$ was shown by Peale (*1*) to be a good diagnostic of the state of the core. In Peale's experiment, the three factors on the righthand side are determined from the amplitude of the longitude librations, the C_{22} gravitational harmonic, and a relation applicable if the planet is in a Cassini state, respectively. The latter relation involves the obliquity of the planet and second-degree gravitational harmonic coefficients.
40. S. Stanley, J. Bloxham, W. E. Hutchison, M. T. Zuber, *Earth Planet. Sci. Lett.* **234**, 27 (2005).
41. U. R. Christensen, *Nature* **444**, 1056 (2006).
42. M. H. Heimpel, J. M. Aurnou, F. M. Al-Shamali, N. Gomez Perez, *Earth Planet. Sci. Lett.* **236**, 542 (2005).
43. S. C. Solomon *et al.*, *Planet. Space Sci.* **49**, 1445 (2001).
44. Images from the spacecraft will also refine estimates of the amount of radial contraction sustained by Mercury. The existence of a partially liquid core may explain why compressional features on the surface appear to accommodate only 1 to 2 km of radial contraction, which is an order of magnitude less than predicted for complete core solidification (*55*).
45. J. S. Lewis, *Earth Planet. Sci. Lett.* **15**, 286 (1972).
46. S. A. Hauck, A. J. Dombard, R. J. Phillips, S. C. Solomon, *Earth Planet. Sci. Lett.* **222**, 713 (2004).
47. J. M. Wahr, *Annu. Rev. Earth Planet. Sci.* **16**, 231 (1988).
48. I. I. Shapiro, S. H. Zisk, A. E. E. Rogers, M. A. Slade, T. W. Thompson, *Science* **178**, 939 (1972).
49. J. L. Margot, D. B. Campbell, R. F. Jurgens, M. A. Slade, *Science* **284**, 1658 (1999).
50. N. J. S. Stacy, thesis, Cornell University, Ithaca, NY (1993).
51. M. Born, E. Wolf, *Principles of Optics* (Cambridge Univ. Press, 1997).
52. J. K. Harmon, M. A. Slade, *Science* **258**, 640 (1992).
53. J. K. Harmon *et al.*, *Nature* **369**, 213 (1994).
54. C. H. De Vries, J. K. Harmon, *Am. Astron. Soc. Meet.* **26**, 1376+ (1994).
55. S. C. Solomon, *Icarus* **28**, 509 (1976).

56. We thank J. Giorgini, A. Behrozi, J. Jao, R. Rose, J. Van Brimmer, D. Choate, D. Kelley, C. Franck, L. Juare, C. Bignell, F. Ghigo, M. Stennes, and R. Maddalena for assistance with the observations; J. Wisdom, D. Stevenson, D. Campbell, M. Standish, M. Yseboodt, J. Hilton, B. Bills, O. Aharonson, S. Stanley, J. Aurnou, S. Hauck, and S. Solomon for insightful discussions; P. Nicholson, S. Ostro, P. Taylor, and two reviewers for comments that improved the manuscript; and NASA's Navigation and Ancillary Information Facility for software and support. The National Radio Astronomy Observatory is a facility of NSF operated under cooperative agreement by Associated Universities, Inc. The Arecibo Observatory is part of the National Astronomy and Ionosphere Center, which is operated by Cornell University under a cooperative agreement with NSF. Part of this work was supported by JPL, operated by Caltech under contract with NASA. This material is based in part on work supported by NASA under the Science Mission Directorate Research and Analysis Programs. S.J.P. is supported in part by the NASA Planetary Geology and Geophysics program under grant NNG05GK58G. J.L.M. is supported in part by the NASA Planetary Astronomy program under grant NNG05GG18G.

29 January 2007; accepted 27 March 2007
10.1126/science.1140514